Title page

Cooperation between Nodal and FGF signals regulates zebrafish cardiac cell migration and heart morphogenesis

Vanessa Gonzalez[1†], Meagan G. Grant[1†], Makoto Suzuki[2], Briana Christophers[1], Jessica Rowland Williams[1#], Rebecca D. Burdine[1*]

[1] Department of Molecular Biology, Princeton University, Princeton, New Jersey, USA, 08544

[2] Amphibian Research Center, Graduate School of Integrated Sciences for Life, Hiroshima University, Higashihiroshima, Hiroshima, Japan, 739-8526.

[#] Current affiliation: National Institute for Student Success, at Georgia State University, Atlanta, GA 30303

[†]**These authors contributed equally to this work**

***Correspondence should be addressed to this author at rburdine@princeton.edu**

Running Title: Nodal & FGF in Cardiac Morphogenesis

Key words: congenital heart defects, left-right asymmetry, cardiac looping, cardiac jogging, Nodal, FGF

Summary statement

This study explores the cooperative and independent roles of Nodal and FGF signaling in generating heart asymmetry.

Abstract

Asymmetric vertebrate heart development is driven by an intricate sequence of morphogenetic cell movements, the coordination of which requires precise interpretation of signaling cues by heart primordia. Here we show that Nodal functions cooperatively with FGF during heart tube formation and asymmetric placement. Both pathways act as migratory stimuli for cardiac progenitor cells (CPCs), but FGF is dispensable for directing heart tube asymmetry, which is governed by Nodal. We further find that Nodal controls CPC migration by inducing left-right asymmetries in the formation of actin-based protrusions in CPCs. Additionally, we define a developmental window in which FGF signals are required for proper heart looping and show cooperativity between FGF and Nodal in this process. We present evidence FGF may promote heart looping through addition of the secondary heart field. Finally, we demonstrate that loss of FGF signaling affects proper development of the atrioventricular canal (AVC), which likely contributes to abnormal chamber morphologies in FGF-deficient hearts. Together, our data shed insight into how the spatiotemporal dynamics of signaling cues regulate the cellular behaviors underlying organ morphogenesis.

Introduction

Vertebrate heart development requires the faithful execution of intricate and successive cell movements. The coupling of these movements to morphogenesis is mediated by the precise interpretation of signaling cues by heart primordia. Perturbations in these signaling pathways can underlie cellular processes that go awry in the roughly 40,000 infants born with a congenital heart defect (CHD) each year in the United States (Tsao et al., 2022). Therefore, a comprehensive analysis of signaling cues that direct cardiac cell behavior is critical for understanding the pathogenic mechanisms of CHDs.

The presence of conserved molecular mechanisms, the amenability to genetic manipulation and live imaging, and the ability for continued embryonic development in the presence of heart defects make zebrafish particularly advantageous for studying the cellular behaviors underlying cardiac morphogenesis (Bakkers, 2011; Genge et al., 2016; Grant et al., 2017; Nguyen et al., 2008; Smith and Uribe, 2021). During the initial stages of zebrafish heart development, cardiac progenitor cells (CPCs) are organized bilaterally within the anterior lateral plate mesoderm (LPM) as epithelial sheets, with ventricular precursors positioned medial to atrial cells. These sheets converge on the embryonic midline, where they form the cardiac cone, a disc-shaped structure comprised of atrial cells at its base and ventricular cells at its apex (19 hours post fertilization, hpf; Bakkers, 2011; Grant et al., 2017; Smith and Uribe, 2021).

During a process known as cardiac jogging, CPCs migrate in a leftward and anterior direction, with cells on the left half of the cardiac cone migrating more rapidly than the right-sided cells (20-24 hpf). This asymmetry in migration velocities results in clockwise rotation of the cardiac cone and displacement of atrial cells to the left and anterior of ventricular cells as the heart tube elongates. Cardiac jogging culminates in the asymmetric placement of the heart tube to the left of the embryonic midline, establishing the first asymmetry in the heart (Baker et al., 2008; de Campos-Baptista et al., 2008; Kidokoro et al., 2022; Lenhart et al., 2013; Rohr et al., 2008; Smith et al., 2008; Veerkamp et al., 2013). Between 30-48 hpf, the heart undergoes an evolutionarily conserved process known as cardiac looping. During this process, the heart tube bends rightward to begin defining and aligning the atrial and ventricular chambers of the heart, with actin polymerization being critical for dictating looping chirality (Desgrange et al., 2018; Noel et al., 2013; Smith and Uribe, 2021). Along with cardiac looping, the cardiac chambers undergo expansion and become morphologically discernible from one another via cardiac ballooning. Regionalized differences in cell morphology bring about chamber formation, and blood flow and contractility are critical for regulating these morphologies (Auman et al., 2007; Dietrich et al., 2014; Smith and Uribe, 2021).

Left-sided Nodal signaling in the LPM governs asymmetric behaviors during jogging and dextral looping of the heart. Nodal directs the asymmetric migration of CPCs during cardiac jogging by increasing the velocities of left-sided cells in the cardiac cone and properly positioning the heart to the

left of the embryonic midline (Baker et al., 2008; de Campos-Baptista et al., 2008; Kidokoro et al., 2022; Lenhart et al., 2013; Rohr et al., 2008; Veerkamp et al., 2013). While looping of the jogged heart tube involves intrinsic mechanisms (Noel et al., 2013), this process is influenced by earlier Nodal signaling to produce robustness in dextral looping morphogenesis (Grimes et al., 2020).

Although Nodal signaling is the dominant signal for sidedness, it is well-established that Nodal signals integrate with other signaling pathways to orchestrate events controlling organogenesis (Hill, 2016; Massague, 2003). For example, during cardiac cone rotation and subsequent jogging, Nodal and BMP signals act synergistically to influence cell migration (Lenhart et al., 2013; Veerkamp et al., 2013). How other signaling pathways potentially cooperate with Nodal signaling to direct asymmetric heart morphogenesis remains uncharacterized.

Here, we characterize the cooperative and independent functions of Nodal and FGF signaling during asymmetric morphogenesis of the zebrafish heart. We find that FGF signaling is required during cardiac jogging as a migratory stimulus for CPCs but is dispensable for determining heart tube laterality. We use confocal live cell imaging to analyze metrics of cell migration and find that aberrant FGF and Nodal signaling alters the velocity dynamics of CPC migration during cone rotation. We also demonstrate that Nodal signals generate sidedness by directing left-right asymmetric protrusive F-actin activity in CPCs. We reveal roles for FGF signaling in promoting proper chamber placement during cardiac looping and show FGF and Nodal signaling cooperate in this process. We provide evidence that the role of FGF in cardiac looping may be through promoting secondary heart field (SHF) addition to the ventricle, suggesting SHF promotes proper looping *in vivo*. Finally, we provide evidence that FGF signaling prior to looping is required for proper development of the atrioventricular canal (AVC). Together, these findings shed insight into how Nodal and FGF signals cooperate to ensure proper migration and morphogenesis in the heart at multiple stages.

Results

FGF and Nodal signals function synergistically during heart tube formation

Previous studies have revealed that the left-sided activation of Nodal within the anterior LPM produces directional migration of CPCs and thus determines the direction of heart tube displacement from the embryonic midline during cardiac jogging (Baker et al., 2008; de Campos-Baptista et al., 2008; Kidokoro et al., 2022; Lenhart et al., 2013; Rohr et al., 2008; Veerkamp et al., 2013). To elucidate mechanisms by which Nodal induces left-right asymmetries in CPC migration rates, we mined our previous microarray studies identifying cardiac-specific transcriptional targets of Nodal. We found a number of components of the FGF signaling pathway as being upregulated by Nodal signals, including FGF ligands, transcriptional targets, and three of four tyrosine kinase receptors (FGFRs; Williams, 2015). Interestingly, various genes involved in FGF signaling have been previously identified as Nodal

targets in zebrafish, including *fgf17b*, *fgf3*, and *fgf8* (Bennett et al., 2007), and *fgf8* is expressed in the cardiac cone prior to cardiac jogging (Fig. 1A; Reifers et al., 1998; Reifers et al., 2000).

To explore the function of FGF signals during heart development, we administered the pan-FGFR inhibitor SU5402 (Mohammadi et al., 1997). Because inhibition of FGF signaling can affect cardiac precursor development (Felker et al., 2018; Marques et al., 2008; Reifers et al., 2000), the use of SU5402 enables precise temporal control over the inhibition of FGF signaling after CPC specification. The addition of SU5402 at 24 hpf resulted in various cardiac defects, including severe pericardial edema and aberrant chamber placement, implicating a role for FGF in asymmetric cardiac morphogenesis (Fig. 1B).

To confirm that treatment with SU5402 did not affect the expression of left-right patterning genes, we analyzed the effect of inhibiting FGF signaling at 18.5 hpf on expression of the Nodal target gene *lefty2* in the cardiac cone. *lefty2* expression serves as both a readout of Nodal responsiveness and a direct readout of the sidedness of Nodal in the embryo (Fig. 1C). In WT embryos, *lefty2* expression was restricted to the left in the cardiac cone, as expected (Fig. 1D). *spaw* mutants lacked *lefty2* expression (Grimes et al., 2020; Noel et al., 2013), while the majority of *ntl* mutants expressed *lefty2* bilaterally (Amack and Yost, 2004), as expected (Fig. 1D). Loss of FGF signaling in SU5402-treated WT embryos did not alter the left-sidedness of Nodal target *lefty2*, nor did loss of FGF change the expression profile of *lefty2* in *spaw* and *ntl* mutants (Fig. 1D), suggesting that any effect of FGF on asymmetric chamber placement was downstream of left-right axis establishment.

To explore the function of FGF signals during cardiac jogging, the first morphological break in symmetry in the embryo, we administered SU5402 at 18.5 hpf, just before the formation of the cardiac cone, and continued treatment until assessment at 24 hpf (Fig. 2A), a time at which most wild-type (WT) embryos have completed extension of the cardiac cone into a linear heart tube (Fig. 2B). As expected, most WT embryos had completed migration and jogging (Fig. 2C). *no tail* (*ntl/ta*) mutants, which have bilateral Nodal expression in the LPM (Amack and Yost, 2004), exhibited only a slight delay in cone-to-tube transition, with most embryos having completed jogging at this time point (Fig. 2C). By contrast, *southpaw* (*spaw*) mutants, which lack Nodal expression in the LPM (Grimes et al., 2020; Noel et al., 2013), displayed a significant delay in tube formation with the majority of hearts remaining at cone stage or starting to extend (Fig. 2C). SU5402-treated WT embryos also experienced a significant delay in tube formation, suggesting a role for FGF signaling in promoting CPC motility in this process (Fig. 2C). Interestingly, treating *ntl* and *spaw* mutants with SU5402 significantly increased delays in tube formation, with most hearts remaining in the cardiac cone stage (Fig. 2C). The strongest effect was observed in *spaw* mutants treated with SU5402, in which all hearts of embryos analyzed remained at the cardiac cone stage at 24 hpf (Fig. 2C). While heart tube formation was delayed at 24 hpf in SU5402-treated and mutant embryos, heart tubes eventually formed in all groups after several additional hours (Fig. 2D,F). Heart tubes were significantly shorter in SU5402-treated embryos, likely

due to inhibition of SHF addition as previously reported (Fig. 2D; de Pater et al., 2009; Felker et al., 2018; Lazic and Scott, 2011). Heart tubes were also shorter in *ntl* and *spaw* mutants, suggesting that elongation is impacted in these mutants or that elongating in a midline position may be inhibited by surrounding tissues (Fig. 2D).

To determine if inhibiting FGF signaling causes defects in cardiac laterality, we examined the direction of heart jogging in embryos with extended heart tubes at 26.5 hpf (Fig. 2E). In WT embryos, heart tubes were displaced to the left of the embryonic midline, producing the expected “left jog” (Fig. 2F). *spaw* mutants and *ntl* mutants exhibited primarily “midline jog”, in which the heart tube fails to be displaced to either side of the midline, as expected (Fig. 2F). Though inhibiting FGF signaling affected the dynamics of heart tube formation, hearts consistently jogged correctly to the left (Fig. 2F), suggesting that FGF signaling is dispensable for instructing cardiac laterality at this point. Overall, this suggests that Nodal and FGF signaling cooperate to promote cell migration during jogging, while only Nodal signaling is required to induce lateralized migration during this process.

Nodal and FGF signals regulate the velocity dynamics and directionality of CPCs during heart tube formation

Perturbation of the Nodal and FGF pathways resulted in defects in heart tube morphogenesis that we hypothesized were due to defects in cell migration. To explore this possibility, we conducted confocal live imaging of embryos that express EGFP under the cardiac-specific *myl7* promoter (Huang et al., 2003) to quantify metrics of cell migration (Fig. 3A). Starting from the formation of the cardiac cone, cell movements were analyzed for three hours in each condition. WT embryos completed jogging within the three-hour time frame and formed a left-lateralized heart tube (Fig. 3B; Movie S1). *ntl* mutants completed jogging in the same time frame but produce midline jogged heart tubes due to bilateral Nodal expression (Fig. 3B; Movie S2). *spaw* mutants also display midline jogging; however, these CPCs migrated more slowly compared to WT or *ntl* mutants, often resulting in incomplete tube extension during the three-hour time frame (Fig. 3B; Movie S3). Similarly, CPCs in SU5402-treated WT embryos migrated more slowly compared to WT or *ntl* mutants, resulting in incomplete tube extension during the imaging time frame (Fig. 3B; Movie S4). Intriguingly, CPCs in SU5402-treated *spaw* mutants scarcely migrated during the same time frame and exhibited a severe delay in heart tube formation (Fig. 3B; Movie S5). These results indicate that FGF signaling acts as a CPC migration stimulus during jogging and acts cooperatively with Nodal in this process.

To better characterize asymmetric migration during jogging, we quantified the trajectories of CPCs by tracking them throughout the duration of the time-lapse movies (Fig. 3C). As the outermost atrial cells of the cardiac cone display the largest disparity in left-right migration rates, we analyzed the movements of this population; the brighter, inner ventricular cells were not included in our analysis. Analysis of the direction and magnitude of CPC trajectories revealed that CPCs in WT embryos

exhibited a marked anterior and leftward displacement, while CPCs in *ntl* and *spaw* mutants failed to undergo strong left or right displacement (Fig. 3D). Furthermore, in *ntl* and *spaw* mutants, overall anterior displacement of CPCs was decreased (Fig. 3D). SU5402-treated embryos displayed a leftward bias, though the overall displacement was not as marked as in WT embryos, and anterior migration was reduced in these embryos (Fig. 3D). Lateral and anterior migrations were most severely disrupted in SU5402-treated *spaw* mutants, further confirming that Nodal and FGF signals work cooperatively to promote CPC migration during jogging (Fig. 3D). The CPC trajectories further suggest that Nodal and FGF signals contribute to the general anterior migration of the heart during jogging, while asymmetric Nodal signals promote lateral migration.

To better understand how Nodal and FGF signals contribute to cardiac laterality, we analyzed the migration velocities of CPCs. Cardiac laterality is known to be directed by left-right biases in cell migration velocity driven by Nodal signaling, with left CPCs displaying a higher velocity that right CPCs in WT embryos (de Campos-Baptista et al., 2008; Kidokoro et al., 2022; Lenhart et al., 2013; Veerkamp et al., 2013). We found that only in WT embryos did strong asymmetric migration velocities exist, with left-sided cardiac cone cells exhibiting significantly higher velocities than right-sided cells (Fig. 3E). Given the bilateral exposure to Nodal of CPCs in *ntl* mutants, we expected migration to be increased on both sides of the cardiac cone as we observed in *ntl* morphants (Lenhart K. F. et al., 2013). However, we found that *ntl* mutants did not display increased migration velocities compared to WT; nevertheless, the expected symmetry in migration velocities was observed (Fig. 3E). Consistent with previous findings (de Campos-Baptista et al., 2008; Kidokoro et al., 2022; Lenhart et al., 2013; Veerkamp et al., 2013), migration velocities of CPCs in *spaw* mutants are symmetric and reduced compared to WT (Fig. 3E). Treatment with SU5402 in WT embryos produced a pronounced reduction of migration velocity similar to that of *ntl* and *spaw* mutants (Fig. 3E). We did observe weak asymmetry in left versus right migration velocities, as is expected given these heart tubes jog correctly to the left and Nodal expression is unaffected in these embryos (Fig. 1D, 2F, 3E). However, the differences in left versus right velocities were not statistically significant in this analysis. Intriguingly, SU5402-treated *spaw* mutants had a more severe reduction in migration velocity compared to *spaw* mutants or SU5402-treated embryos, further suggesting cooperation between Nodal and FGF signals in this process (Fig. 3E). Taken together, our findings on CPC migration, velocity, and trajectories all support Nodal acting to bias left migration velocities, while FGF acts with Nodal to promote overall CPC velocities during heart tube morphogenesis.

Nodal elicits left-right asymmetries in migration by inducing left-right asymmetries in actin polymerization in CPCs

Though previous studies have elucidated a role for the Nodal pathway in governing cardiac laterality, the molecular mechanisms by which the pathway does so remain unclear. A promising

possibility is that Nodal promotes cell migration by asymmetrically influencing the actin cytoskeleton and its regulators during cardiac jogging. It is known that actin can be regulated by Nodal signaling during cardiac looping and in other developmental contexts (Noel et al., 2013; Woo et al., 2012). Furthermore, FGF signaling is also known to regulate cytoskeletal dynamics, including actin polarization (Sai and Ladher, 2008; Yang et al., 2020). To assess this possibility, we generated *Tg*(*myl7:Lifeact-EGFP*) fish, in which EGFP-labeled filamentous actin (F-actin) is restricted to CPCs (Huang et al., 2003; Reischauer et al., 2014; Riedl et al., 2008), permitting us to observe F-actin levels and cellular protrusive activity (Fig. 4A). Two-photon imaging of the cardiac cone in WT Lifeact-EGFP transgenics revealed left-sided atrial cells have higher levels of F-actin than the corresponding right-sided cells, and this asymmetry in F-actin persisted throughout jogging (Fig. 4B; Movie S6). Imaging injected embryos mosaically expressing Lifeact-EGFP at the cellular level revealed numerous Lifeact-EGFP-positive protrusions in left-sided atrial cells where motility rates are high (Fig. 4C; Movie S7).

To determine if the higher F-actin levels we observe in left atrial cells are in response to Nodal signaling, we examined actin dynamics in *ntl* morphants, in *spaw* morphants, and in embryos treated with SB-505124, a pharmacological inhibitor of Nodal signaling that works well in zebrafish (DaCosta Byfield et al., 2004; Hagos and Dougan, 2007). In WT embryos, left-sided CPCs exhibited high levels of F-actin (Fig. 4D). No increase in F-actin levels in atrial cells was observed when Nodal signaling was lost in *spaw* morphants or with administration of SB-505124 (Fig. 4D; Movies S8-9). Conversely, we observed a symmetrical increase in F-actin level in *ntl* morphants, in which Nodal is expressed bilaterally in the LPM (Fig. 4D; Movie S10). To quantify these results, we measured the ratio of fluorescence intensity values between left-sided and right-sided cells (Fig. 4E). An intensity ratio of left-to-right cells greater than 1 is indicative of left-biased levels, while an intensity ratio equal to 1 indicates symmetric levels. We found the fluorescence intensity ratio in WT embryos to be left-biased, which is indicative of asymmetric F-actin levels (Fig. 4F). However, *ntl* morphants, *spaw* morphants, and SB505124-treated embryos had ratios indicative of symmetric F-actin levels (Fig. 4F). Taken together, these findings support our hypothesis that Nodal induces left-right asymmetries in migration velocity by promoting actin cytoskeleton dynamics.

FGF signaling is necessary for cardiac looping

FGF signaling is known to influence various aspects of zebrafish heart morphogenesis, such as CPC differentiation and proliferation, as well as chamber size and identity establishment (de Pater et al., 2009; Felker et al., 2018; Lazic and Scott, 2011; Marques et al., 2008; Pradhan et al., 2017; Reifers et al., 1998; Zeng and Yelon, 2014). In embryos treated with SU5402 from 24-48 hpf (continuous treatment; Fig. 5A), differences in heart tube morphology between treated and vehicle-treated embryos are apparent. SU5402-treated embryos exhibit defects in heart looping, chamber shape, and ventricle size, as reported previously (Fig. 5B). Given the ostensible importance of FGF signaling in heart

looping, the second and more evolutionarily conserved asymmetry in heart development, we wanted to determine if there was a more specific developmental window in which FGF signaling influences this process.

To further investigate the role of FGF in cardiac looping, we treated embryos with SU5402 during more specific developmental windows: during the heart tube elongation phase (24-30 hpf, prior to the onset of looping) and the heart tube bending phase (30-36 hpf, during looping; Fig. 5A). In vehicle-treated embryos, the heart has completed looping and the atrium and ventricle are positioned side-by-side at 48 hpf (Fig. 5B). Treatment during both of our defined developmental windows resulted in a vertically “stacked” chamber phenotype indicative of looping defects (Fig. 5B). Quantification of these chamber placement defects was conducted by measuring the looping angle: the angle formed by the intersection of a line along the anterior-posterior axis and a line through the atrioventricular canal (AVC) at 48 hpf, with a properly developed heart having a looping angle of ~25.0° (Chernyavskaya et al., 2012). We found that SU5402 treatment during the elongation phase resulted in significantly larger looping angles (mean looping angle = 41.2°), suggesting impaired looping, while treatment during the bending phase was not significantly different than WT (Fig. 5C). This suggests FGF signaling between 24 to 30 hpf is important for proper heart looping. Heart looping is compromised in *spaw* mutants (Fig. 5C; mean looping angle = 65.1°), and we find loss of FGF signaling during the elongation phase in *spaw* mutants exacerbates heart looping defects (Fig. 5C; mean looping angle 74.6°). Our results suggest that Nodal and FGF cooperate to promote heart looping.

SHF addition is required for heart looping

Others have shown that loss of FGF signaling post 24 hpf prevents addition of the secondary heart field (SHF) to the arterial pole of the heart tube. To determine if our treatment with SU5402 affected SHF addition during the elongation phase, we treated embryos starting at 24 hpf and imaged the heart tube at both 26.5 and 28 hpf. Measuring heart tube length revealed significantly shorter heart tubes in SU5402-treated embryos (Fig. 5D), indicative of loss of the SHF. This suggested to us that the addition of SHF cells is critical for proper heart looping. To address this possibility, we injected embryos at the 1-cell stage with a morpholino against *ltbp3*, a canonical SHF marker that is necessary for SHF addition to the heart tube (Zhou et al., 2011), and assessed the heart at 48 hpf. *ltbp3* morphants exhibited looping and chamber placement defects similar to SU5402-treated embryos (Fig. 6A). Quantification revealed the looping angle in morphants was significantly higher (mean looping angle = 51.1°) than in vehicle-injected embryos (mean looping angle = 25.8°; Fig. 6B). This indicates that addition of SHF cells to the heart tube is needed for proper cardiac looping *in vivo*.

Loss of FGF signaling during elongation and bending phases compromises AVC development

SU5402 treatment during the elongation and bending phases produced aberrant chamber morphologies with smaller ventricles and elongated atria (Fig. 5B). Intriguingly, it is known that *nppa/nppb* double mutants exhibit abnormal atrial morphologies due to errors in AVC development; AVC defects result in improper blood flow, which in turn cause defects in chamber ballooning (Auman et al., 2007; Dietrich et al., 2014; Grassini et al., 2018). To determine if FGF inhibition influences AVC development, we analyzed expression of *nppa*. *nppa* is typically expressed in the outer curvatures of the heart chambers but is excluded from the AVC, a phenotype observed in vehicle-treated embryos (Fig. 6C-D). In SU5402-treated embryos, *nppa* was expressed in the AVC, which is an abnormal *nppa* expression pattern (Fig. 6C-D). Overall, these findings suggest that FGF signaling may influence chamber morphology by promoting proper formation of the AVC.

Discussion

Nodal and FGF signals function synergistically to promote migration underlying cardiac jogging and tube extension

Our results show that Nodal and FGF signals cooperatively promote overall cell migration during heart tube formation and asymmetric placement. Losing either signal reduces cell velocities in the cone and delays the cone-to-tube transition compared to WT, while losing both signals more severely perturbs CPC migration and tube formation. Though anterior movement of CPCs is reduced in hearts lacking Nodal or FGF signals, it is not completely abolished, raising the question as to what additional signals govern the anterior migration of CPCs. During jogging, our data suggests that FGF signals act permissively to promote motility, while Nodal signals act instructively to direct CPC laterality. FGF signaling is known to cooperate with Nodal signaling in coupling cell migration in various morphogenetic events, including in the *Ciona* neural tube and the zebrafish brain (Navarrete and Levine, 2016; Regan et al., 2009; Roussigne et al., 2018). Intriguingly, in the zebrafish brain, FGF and Nodal signaling function together to control left-right asymmetry by mediating collective cell migration; Nodal restricts and biases the activation of FGF to leading parapineal cells, resulting in a leftward, asymmetric migration (Regan et al., 2009; Roussigne et al., 2018). Similar to what we report in this paper, while FGF is critical for parapineal cell migration, Nodal signaling directs the laterality of this movement.

We also find that the heart tubes of *spaw* and *ntl* mutants are significantly shorter than those of WT embryos. Whether this defect is only the consequence of compromised motility, or whether there are other forces that restrict elongation, remains to be determined. For example, the defects we observe are highly reminiscent of *heart and mind* (*had*) and *heart and soul* (*has*) mutants, which have reduced heart tube extension (Rohr et al., 2006; Shu et al., 2003). Interestingly, *had* and *has* encode regulators of epithelial polarity, the establishment and maintenance of which is crucial for proper cardiac morphogenesis. Interrogating epithelial polarity and cell shape changes under the conditions in our study may well prove informative in understanding heart tube extension. Alternatively, the decrease

in heart tube length we observe in our study conditions could be due to tissue constraints on the tube as it attempts to elongate closer to the midline. Future studies are needed to determine what drives the overall anterior displacement of the heart cone/tube and the forces that drive tube extension during development.

Nodal signals induce left-right asymmetries in CPCs by impinging on the actin cytoskeleton

To determine the mechanisms by which Nodal regulates asymmetric CPC migration, we imaged actin filament formation during cardiac jogging using a Lifeact reporter. Previous studies have suggested roles for Nodal in inducing cytoskeletal rearrangements in migrating cells (Noel et al., 2013; Schier, 2009; Woo et al., 2012). Here, we link its asymmetric impingement on the actin cytoskeleton to tissue morphogenesis *in vivo*. In wild-type embryos we observe an increase in F-actin in migrating left atrial cells that is not observed in right atrial cells. This increase in F-actin is Nodal dependent, as it is lost in embryos injected with *spaw* morpholino or treated with Nodal inhibitor. In agreement, in embryos injected with *ntl* morpholino, where Nodal signals to both sides of the cardiac cone, both left and right atrial cells show increases in F-actin. This suggests that Nodal induces asymmetric migration by increasing actin dynamics within left-atrial cells, which migrate faster than their counterparts on the right, driving clockwise rotation of the cone. The cells in the cone are epithelial and migrate collectively during jogging. Intriguingly, using mosaic labeling with our Lifeact reporter, we observed highly dynamic, protrusive F-actin activity in these left-sided migrating cells. It is intriguing to speculate that these are “cryptic” basal extensions that are driving migration similar to what has been observed in cultured MDCK kidney cells during wound healing (Farooqui and Fenteany, 2005). Future studies can determine if these protrusions are basal-to-junctional complexes coming only from edge cells or if additional cells deeper in this epithelium are helping drive migration.

FGF signaling is necessary for proper cardiac looping and AVC development

Extending our studies with the FGF inhibitor SU5402, we find that treatment with SU5402 from 24 to 30 hpf (elongation) affected both looping and chamber expansion, while treatment from 30 to 36 hpf (bending) primarily affected chamber expansion. This suggests that FGF continues to play important roles in heart morphogenesis after jogging is complete. Cardiac looping is a highly conserved event in vertebrate heart development, but much remains to be discovered regarding its underlying mechanisms. We previously reported that jogging correctly increases the correct dextral loop in the heart, suggesting that the first asymmetric migration at 20 hpf still provides input to heart-intrinsic chirality mechanisms at later stages (Grimes et al., 2020). Our work here suggests that at least one additional input into looping *in vivo* involves FGF. We provide evidence that this input may be through SHF addition given the similarity in phenotypes between *ltbp3* morphants and SU5402-treated embryos, both of which lack SHF structures. This is further supported by work showing heart looping

defects in *isl2a* and *isl2b* mutant embryos, which produce defects in the SHF (Witzel et al., 2017). Determining how the SHF contributes to proper heart looping in zebrafish will be an important area for future studies. Intriguingly, we show that Nodal and FGF cooperate to promote heart looping, as losing both pathways produces more severe defects in this process than losing either alone.

A requirement for proper blood flow in chamber expansion is clear (Auman et al., 2007; Dietrich et al., 2014); however, the physical forces governing chamber shape remain to be fully determined. We find that inhibiting FGF at elongation or bending phases affects AVC development. In treated embryos, *nppa* expression expands into the AVC region, suggesting that there are defects in specification or differentiation of this structure. Such an issue could lead to defective functioning of the AVC, resulting in aberrant blood flow, improper chamber expansion, and the abnormal chamber shapes we observe. Determining what aspects of cell movements or cell specification are influenced by FGF in the AVC is an area for future studies.

Nodal and FGF signaling are critical for heart morphogenesis

Here, we highlight molecular mechanisms through which the spatiotemporal dynamics of signaling cues influence cardiac precursor cell behaviors and heart morphogenesis. We further show that the differential effects exerted by interacting signals on CPCs manifest as dramatic asymmetries in heart tube morphogenesis, highlighting the fact that earlier patterning events regulate morphogenetic processes occurring later in development. Heart tube malformations are among the most commonly diagnosed congenital heart defects, thus understanding how they arise is crucial for reducing the mortality and morbidity associated with CHDs. Ultimately, further interrogation of the roles of Nodal and FGF signaling throughout heart morphogenesis will prove informative in understanding how signaling and cellular aberrancies manifest as morphological defects.

Materials and methods

Zebrafish strains

All experimental procedures in this study were conducted in accordance with the Princeton University Institutional Animal Care and Use Committee. Zebrafish (*Danio rerio*) embryos were maintained at 28°C and grown in E3 embryo medium (5 mM NaCl, 0.17 mM KCl, 0.33 mM $CaCl_2$, 0.33 mM $MgSO_4$). We used the zebrafish mutants ntl^{b160} and $spaw^{sa177}$ (Grimes et al., 2020; Halpern et al., 1993). We used the transgenic strain *Tg(myl7:EGFP)* (Huang et al., 2003).

Generation of transgenic line

We generated the *Tg(myl7:Lifeact-EGFP)* transgenic strain by using the Tol2 transposase system (Kawakami, 2007). Briefly, 1-cell stage embryos were injected with Tol2 mRNA and *pTol2005b-*

myl7:Lifeact-EGFP plasmid. Only correctly developing embryos with EGFP-positive hearts were raised. Injected F0 fish were outcrossed to generate a stable transgenic line.

Drug treatments and morpholino injections

A 10mM stock of the FGFR inhibitor SU5402 (Sigma-Aldrich) in DMSO was diluted to a working concentration of 6μM or 10μM in a 1% DMSO/1X E3 solution. 6μM was used for inhibition during bending and elongation phases and 10μM was used for inhibition during jogging phase. Embryos were incubated at 28°C in the dark for varying durations of time: 18.5-24 hpf, 24-30 hpf, and 30-36 hpf. Upon completion of SU5402 incubation, embryos underwent live imaging or were fixed in 4% paraformaldehyde (PFA; Electron Microscopy Sciences) for RNA *in situ* analysis. Due to the light-sensitivity of SU5402, treated embryos were incubated in the dark. For SB-505124 (Sigma-Aldrich) treatments, a 10mM stock in DMSO was diluted to a working concentration of 40 μM and administered to embryos at the tailbud stage; embryos then underwent live imaging during jogging as described (Lenhart et al., 2013). Note that DMSO-treated vehicles did not differ from WT embryos in the processes studied. Morpholino injections were performed as previously described using established morpholinos for *spaw*, *ntl*, and *ltbp3* (Lenhart et al., 2013; Long et al., 2003; Nasevicius and Ekker, 2000; Zhou et al., 2011).

RNA *in situ* hybridization

Chromogenic whole-mount RNA *in situ* hybridization was performed using digoxygenin-labelled RNA probes for *myl7*, *lefty2*, and *nppa* (Berdougo et al., 2003; Bisgrove et al., 1999; Thisse and Thisse, 2014; Yelon et al., 1999). Images were acquired using the Leica DMRA microscope. Fluorescent whole-mount *in situ* hybridization was performed using the Molecular Instruments HCR kit as described (Choi et al., 2018) for probes against *myl7* and *fgf8*. Images were acquired using the Nikon A1 confocal microscope.

Live imaging and analysis

To analyze cell migration during cardiac jogging, dechorionated embryos were mounted in 0.8% low-melt agarose as previously described (Lenhart et al., 2013). The dish was covered with a 0.5% DMSO/1X E3 solution containing 0.13mM tricaine (MS-222; Sigma-Aldrich). For SU5402 treatments, a 5 μM dilution in 0.8% agarose was used for mounting embryos, which were incubated in inhibitor at least 30 minutes before mounting and covered with 10μM inhibitor in 0.5% DMSO/1X E3 containing 0.13mM tricaine.

For analysis of cardiac cell movements, embryos were imaged from 18-24 hpf using a Leica SP5 confocal microscope. The Leica Mark & Find feature was used to image up to 4 embryos per

imaging session for higher throughput. A heated stage set to 28.5°C was used, which permitted imaging for several hours without perturbing development.

We acquired confocal z-stacks at 4- or 5-minute intervals with a spacing of 2 µm. To track individual cells during jogging, we compressed the z-stacks into a single dimension and then utilized the ImageJ program TrackMate to track and quantify metrics of each cell during its migration. To ensure consistent quantification of velocity over time between different genotypes, we tracked CPCs over the same developmental window: we began tracking cells upon anterior fusion of CPCs at the midline and ended tracking 3 hours thereafter. Note that only outer, atrial cells were chosen for tracking as they undergo the most migration during jogging; the bright ventricular cells around the lumen are excluded from analysis (Lenhart et al., 2013). Average velocity and angle of displacement for each cell was calculated using raw position, displacement, and time measurements generated by TrackMate. Resulting cell velocities, angles, and displacements were input into Prism or RStudio for analysis. Note that distinct microscopes, acquisition parameters, and analysis software were utilized and may account for differences in velocity values, compared to our previous publications.

We note that the decreased velocity we observe here in *ntl* mutants conflicts with our previously published data using *ntl* morphants, in which we observed higher velocities in CPCs compared to WT (Lenhart et al., 2013). It is possible that there may be an unexpected difference in *ntl* mutants versus morphants that produces this discrepancy (Stainier et al., 2017). However, distinct microscopes, acquisition parameters, and analysis software were utilized in this study and could also account for differences in velocity values, compared to our previous publication.

For two-photon analysis of protrusive F-actin activity, embryos were mounted and handled as described above. Embryos were imaged from 19-23 hpf using a Prairie Ultima two-photon microscope. Z-stacks were acquired at 15-minute intervals with a spacing of 4 µm. Fluorescence intensity analysis was performed using ImageJ.

For observing heart tube length and cardiac looping, embryos were mounted and handled as described above. Images were acquired using the Leica M205 FA fluorescent stereoscope. Analysis was performed using ImageJ as described previously or below.

Heart measurements

For fixed embryos processed via RNA *in situ* hybridization, heart tube length was measured using the ruler tool in Photoshop or ImageJ. For observing heart tube length and cardiac looping in live embryos, embryos were mounted and handled as described above. Images were acquired using the Leica M205 FA fluorescent stereoscope. Analysis was performed using ImageJ ruler and angle tools. The looping angle is defined as the angle between the plane of the anterior-posterior axis and the AVC (Chernyavskaya et al., 2012).

Statistical analysis

All bar graphs were generated using GraphPad Prism 9.4.0. Statistical tests of significance (Student's t-test, Chi-square analysis) were calculated using GraphPad Prism analysis software.

Acknowledgements

We would like to thank Dr. Gary Laevsky and the Confocal Imaging Facility, a Nikon Center of Excellence, in the Department of Molecular Biology for their assistance with imaging. We also thank Phillip Johnson and his team for their assistance with fish husbandry.

Competing Interests

The authors declare that they have no conflict of interest.

Funding

M.S. was a visiting scientist supported by the Strategic International Research Exchange Program between Princeton University and National Institutes of Natural Sciences, Japan. Research reported in this manuscript was supported by a National Science Foundation under grant IOS-1147123 to RDB and a predoctoral fellowship to JRW; a Janssen Scholars of Oncology Diversity Engagement Fellowship to VG; grant R01HD048584 from the National Institutes of Child Health and Human Development to RDB, and grant T32GM007388 from the National Institute of General Medical Sciences to JRW. The content is solely the responsibility of the authors and does not necessarily represent the official views of the National Institutes of Health.

Data availability

The data that support the findings of this study are available from the corresponding author RDB, upon reasonable request.

Diversity and inclusion statement

One or more of the authors of this paper self-identifies as an underrepresented ethnic minority in science. One or more of the authors of this paper self-identifies as living with a disability. One or more authors of this paper received support from a program designed to increase minority representation in science. Five of the six authors on this paper are women who are often underrepresented in science.

References

Amack, J. D. and Yost, H. J. (2004). The T box transcription factor no tail in ciliated cells controls zebrafish left-right asymmetry. *Curr Biol* **14**, 685-690.

Auman, H. J., Coleman, H., Riley, H. E., Olale, F., Tsai, H. J. and Yelon, D. (2007). Functional modulation of cardiac form through regionally confined cell shape changes. *PLoS Biol* **5**, e53.

Baker, K., Holtzman, N. G. and Burdine, R. D. (2008). Direct and indirect roles for Nodal signaling in two axis conversions during asymmetric morphogenesis of the zebrafish heart. *Proc Natl Acad Sci U S A* **105**, 13924-13929.

Bakkers, J. (2011). Zebrafish as a model to study cardiac development and human cardiac disease. *Cardiovasc Res* **91**, 279-288.

Bennett, J. T., Joubin, K., Cheng, S., Aanstad, P., Herwig, R., Clark, M., Lehrach, H. and Schier, A. F. (2007). Nodal signaling activates differentiation genes during zebrafish gastrulation. *Dev Biol* **304**, 525-540.

Berdougo, E., Coleman, H., Lee, D. H., Stainier, D. Y. and Yelon, D. (2003). Mutation of weak atrium/atrial myosin heavy chain disrupts atrial function and influences ventricular morphogenesis in zebrafish. *Development* **130**, 6121-6129.

Bisgrove, B. W., Essner, J. J. and Yost, H. J. (1999). Regulation of midline development by antagonism of lefty and nodal signaling. *Development* **126**, 3253-3262.

Chernyavskaya, Y., Ebert, A. M., Milligan, E. and Garrity, D. M. (2012). Voltage-gated calcium channel CACNB2 (beta2.1) protein is required in the heart for control of cell proliferation and heart tube integrity. *Dev Dyn* **241**, 648-662.

Choi, H. M. T., Schwarzkopf, M., Fornace, M. E., Acharya, A., Artavanis, G., Stegmaier, J., Cunha, A. and Pierce, N. A. (2018). Third-generation in situ hybridization chain reaction: multiplexed, quantitative, sensitive, versatile, robust. *Development* **145**.

DaCosta Byfield, S., Major, C., Laping, N. J. and Roberts, A. B. (2004). SB-505124 is a selective inhibitor of transforming growth factor-beta type I receptors ALK4, ALK5, and ALK7. *Mol Pharmacol* **65**, 744-752.

de Campos-Baptista, M. I., Holtzman, N. G., Yelon, D. and Schier, A. F. (2008). Nodal signaling promotes the speed and directional movement of cardiomyocytes in zebrafish. *Dev Dyn* **237**, 3624-3633.

de Pater, E., Clijsters, L., Marques, S. R., Lin, Y. F., Garavito-Aguilar, Z. V., Yelon, D. and Bakkers, J. (2009). Distinct phases of cardiomyocyte differentiation regulate growth of the zebrafish heart. *Development* **136**, 1633-1641.

Desgrange, A., Le Garrec, J. F. and Meilhac, S. M. (2018). Left-right asymmetry in heart development and disease: forming the right loop. *Development* **145**.

Dietrich, A. C., Lombardo, V. A., Veerkamp, J., Priller, F. and Abdelilah-Seyfried, S. (2014). Blood flow and Bmp signaling control endocardial chamber morphogenesis. *Dev Cell* **30**, 367-377.

Farooqui, R. and Fenteany, G. (2005). Multiple rows of cells behind an epithelial wound edge extend cryptic lamellipodia to collectively drive cell-sheet movement. *J Cell Sci* **118**, 51-63.

Felker, A., Prummel, K. D., Merks, A. M., Mickoleit, M., Brombacher, E. C., Huisken, J., Panakova, D. and Mosimann, C. (2018). Continuous addition of progenitors forms the cardiac ventricle in zebrafish. *Nat Commun* **9**, 2001.

Genge, C. E., Lin, E., Lee, L., Sheng, X., Rayani, K., Gunawan, M., Stevens, C. M., Li, A. Y., Talab, S. S., Claydon, T. W., et al. (2016). The Zebrafish Heart as a Model of Mammalian Cardiac Function. *Rev Physiol Biochem Pharmacol* **171**, 99-136.

Grant, M. G., Patterson, V. L., Grimes, D. T. and Burdine, R. D. (2017). Modeling Syndromic Congenital Heart Defects in Zebrafish. *Curr Top Dev Biol* **124**, 1-40.

Grassini, D. R., Lagendijk, A. K., De Angelis, J. E., Da Silva, J., Jeanes, A., Zettler, N., Bower, N. I., Hogan, B. M. and Smith, K. A. (2018). Nppa and Nppb act redundantly during zebrafish cardiac development to confine AVC marker expression and reduce cardiac jelly volume. *Development* **145**.

Grimes, D. T., Patterson, V. L., Luna-Arvizu, G., Schottenfeld-Roames, J., Irons, Z. H. and Burdine, R. D. (2020). Left-right asymmetric heart jogging increases the robustness of dextral heart looping in zebrafish. *Dev Biol* **459**, 79-86.

Hagos, E. G. and Dougan, S. T. (2007). Time-dependent patterning of the mesoderm and endoderm by Nodal signals in zebrafish. *BMC Dev Biol* **7**, 22.

Halpern, M. E., Ho, R. K., Walker, C. and Kimmel, C. B. (1993). Induction of muscle pioneers and floor plate is distinguished by the zebrafish no tail mutation. *Cell* **75**, 99-111.

Hill, C. S. (2016). Transcriptional Control by the SMADs. *Cold Spring Harb Perspect Biol* **8**.

Huang, C. J., Tu, C. T., Hsiao, C. D., Hsieh, F. J. and Tsai, H. J. (2003). Germ-line transmission of a myocardium-specific GFP transgene reveals critical regulatory elements in the cardiac myosin light chain 2 promoter of zebrafish. *Dev Dyn* **228**, 30-40.

Kawakami, K. (2007). Tol2: a versatile gene transfer vector in vertebrates. *Genome Biol* **8 Suppl 1**, S7.

Kidokoro, H., Saijoh, Y. and Schoenwolf, G. C. (2022). Nodal signaling regulates asymmetric cellular behaviors, driving clockwise rotation of the heart tube in zebrafish. *Commun Biol* **5**, 996.

Lazic, S. and Scott, I. C. (2011). Mef2cb regulates late myocardial cell addition from a second heart field-like population of progenitors in zebrafish. *Dev Biol* **354**, 123-133.

Lenhart, K. F., Holtzman, N. G., Williams, J. R. and Burdine, R. D. (2013). Integration of nodal and BMP signals in the heart requires FoxH1 to create left-right differences in cell migration rates that direct cardiac asymmetry. *PLoS Genet* **9**, e1003109.

Long, S., Ahmad, N. and Rebagliati, M. (2003). The zebrafish nodal-related gene southpaw is required for visceral and diencephalic left-right asymmetry. *Development* **130**, 2303-2316.

Marques, S. R., Lee, Y., Poss, K. D. and Yelon, D. (2008). Reiterative roles for FGF signaling in the establishment of size and proportion of the zebrafish heart. *Dev Biol* **321**, 397-406.

Massague, J. (2003). Integration of Smad and MAPK pathways: a link and a linker revisited. *Genes Dev* **17**, 2993-2997.

Mohammadi, M., McMahon, G., Sun, L., Tang, C., Hirth, P., Yeh, B. K., Hubbard, S. R. and Schlessinger, J. (1997). Structures of the tyrosine kinase domain of fibroblast growth factor receptor in complex with inhibitors. *Science* **276**, 955-960.

Nasevicius, A. and Ekker, S. C. (2000). Effective targeted gene 'knockdown' in zebrafish. *Nat Genet* **26**, 216-220.

Navarrete, I. A. and Levine, M. (2016). Nodal and FGF coordinate ascidian neural tube morphogenesis. *Development* **143**, 4665-4675.

Nguyen, C. T., Lu, Q., Wang, Y. and Chen, J. N. (2008). Zebrafish as a model for cardiovascular development and disease. *Drug Discov Today Dis Models* **5**, 135-140.

Noel, E. S., Verhoeven, M., Lagendijk, A. K., Tessadori, F., Smith, K., Choorapoikayil, S., den Hertog, J. and Bakkers, J. (2013). A Nodal-independent and tissue-intrinsic mechanism controls heart-looping chirality. *Nat Commun* **4**, 2754.

Pradhan, A., Zeng, X. I., Sidhwani, P., Marques, S. R., George, V., Targoff, K. L., Chi, N. C. and Yelon, D. (2017). FGF signaling enforces cardiac chamber identity in the developing ventricle. *Development* **144**, 1328-1338.

Regan, J. C., Concha, M. L., Roussigne, M., Russell, C. and Wilson, S. W. (2009). An Fgf8-dependent bistable cell migratory event establishes CNS asymmetry. *Neuron* **61**, 27-34.

Reifers, F., Bohli, H., Walsh, E. C., Crossley, P. H., Stainier, D. Y. and Brand, M. (1998). Fgf8 is mutated in zebrafish acerebellar (ace) mutants and is required for maintenance of midbrain-hindbrain boundary development and somitogenesis. *Development* **125**, 2381-2395.

Reifers, F., Walsh, E. C., Leger, S., Stainier, D. Y. and Brand, M. (2000). Induction and differentiation of the zebrafish heart requires fibroblast growth factor 8 (fgf8/acerebellar). *Development* **127**, 225-235.

Reischauer, S., Arnaout, R., Ramadass, R. and Stainier, D. Y. (2014). Actin binding GFP allows 4D in vivo imaging of myofilament dynamics in the zebrafish heart and the identification of Erbb2 signaling as a remodeling factor of myofibril architecture. *Circ Res* **115**, 845-856.

Riedl, J., Crevenna, A. H., Kessenbrock, K., Yu, J. H., Neukirchen, D., Bista, M., Bradke, F., Jenne, D., Holak, T. A., Werb, Z., et al. (2008). Lifeact: a versatile marker to visualize F-actin. *Nat Methods* **5**, 605-607.

Rohr, S., Bit-Avragim, N. and Abdelilah-Seyfried, S. (2006). Heart and soul/PRKCi and nagie oko/Mpp5 regulate myocardial coherence and remodeling during cardiac morphogenesis. *Development* **133**, 107-115.

Rohr, S., Otten, C. and Abdelilah-Seyfried, S. (2008). Asymmetric involution of the myocardial field drives heart tube formation in zebrafish. *Circ Res* **102**, e12-19.

Roussigne, M., Wei, L., Tsingos, E., Kuchling, F., Alkobtawi, M., Tsalavouta, M., Wittbrodt, J., Carl, M., Blader, P. and Wilson, S. W. (2018). Left/right asymmetric collective migration of parapineal cells is mediated by focal FGF signaling activity in leading cells. *Proc Natl Acad Sci U S A* **115**, E9812-E9821.

Sai, X. and Ladher, R. K. (2008). FGF signaling regulates cytoskeletal remodeling during epithelial morphogenesis. *Curr Biol* **18**, 976-981.

Schier, A. F. (2009). Nodal morphogens. *Cold Spring Harb Perspect Biol* **1**, a003459.

Shu, X., Cheng, K., Patel, N., Chen, F., Joseph, E., Tsai, H. J. and Chen, J. N. (2003). Na,K-ATPase is essential for embryonic heart development in the zebrafish. *Development* **130**, 6165-6173.

Smith, K. A., Chocron, S., von der Hardt, S., de Pater, E., Soufan, A., Bussmann, J., Schulte-Merker, S., Hammerschmidt, M. and Bakkers, J. (2008). Rotation and asymmetric development of the zebrafish heart requires directed migration of cardiac progenitor cells. *Dev Cell* **14**, 287-297.

Smith, K. A. and Uribe, V. (2021). Getting to the Heart of Left-Right Asymmetry: Contributions from the Zebrafish Model. *J Cardiovasc Dev Dis* **8**.

Stainier, D. Y. R., Raz, E., Lawson, N. D., Ekker, S. C., Burdine, R. D., Eisen, J. S., Ingham, P. W., Schulte-Merker, S., Yelon, D., Weinstein, B. M., et al. (2017). Guidelines for morpholino use in zebrafish. *PLoS Genet* **13**, e1007000.

Thisse, B. and Thisse, C. (2014). In situ hybridization on whole-mount zebrafish embryos and young larvae. *Methods Mol Biol* **1211**, 53-67.

Tsao, C. W., Aday, A. W., Almarzooq, Z. I., Alonso, A., Beaton, A. Z., Bittencourt, M. S., Boehme, A. K., Buxton, A. E., Carson, A. P., Commodore-Mensah, Y., et al. (2022). Heart Disease and Stroke Statistics-2022 Update: A Report From the American Heart Association. *Circulation* **145**, e153-e639.

Veerkamp, J., Rudolph, F., Cseresnyes, Z., Priller, F., Otten, C., Renz, M., Schaefer, L. and Abdelilah-Seyfried, S. (2013). Unilateral dampening of Bmp activity by nodal generates cardiac left-right asymmetry. *Dev Cell* **24**, 660-667.

Williams, J. R. (2015). Nodal Directs Asymmetric Cardiac Morphogenesis Through Regulation of Actin Cytoskeleton. In *Molecular Biology*. Princeton, NJ: Princeton University.

Witzel, H. R., Cheedipudi, S., Gao, R., Stainier, D. Y. and Dobreva, G. D. (2017). Isl2b regulates anterior second heart field development in zebrafish. *Sci Rep* **7**, 41043.

Woo, S., Housley, M. P., Weiner, O. D. and Stainier, D. Y. (2012). Nodal signaling regulates endodermal cell motility and actin dynamics via Rac1 and Prex1. *J Cell Biol* **198**, 941-952.

Yang, S., Weske, A., Du, Y., Valera, J. M., Jones, K. L. and Johnson, A. N. (2020). FGF signaling directs myotube guidance by regulating Rac activity. *Development* **147**.

Yelon, D., Horne, S. A. and Stainier, D. Y. (1999). Restricted expression of cardiac myosin genes reveals regulated aspects of heart tube assembly in zebrafish. *Dev Biol* **214**, 23-37.

Zeng, X. X. and Yelon, D. (2014). Cadm4 restricts the production of cardiac outflow tract progenitor cells. *Cell Rep* **7**, 951-960.

Zhou, Y., Cashman, T. J., Nevis, K. R., Obregon, P., Carney, S. A., Liu, Y., Gu, A., Mosimann, C., Sondalle, S., Peterson, R. E., et al. (2011). Latent TGF-beta binding protein 3 identifies a second heart field in zebrafish. *Nature* **474**, 645-648.

Figure legends

Figure 1. FGF signaling is active in the developing heart and necessary for proper heart development. (**A**) RNA *in situ* hybridization (ISH) by hybridization chain reaction (HCR) for *fgf8* (magenta) and *myl7* (green) in the cardiac cone of a 20 hours post fertilization (hpf) wild-type (WT) embryo. Scale = 25 µm. (**B**) Representative images of 5 days post fertilization (dpf) embryos treated

with vehicle or FGF inhibitor SU5402 from 24-30 hpf (ventricle in magenta, atrium in cyan). SU5402-treated embryos display aberrant cardiac looping, blood pooling at the sinus venosus, and pericardial edema (lateral view) as well as the atrium failing to migrate behind the ventricle (ventral view). (**C**) ISH for Nodal target gene *lefty2* in the cardiac cone of 20 hpf embryos shows correct left-sided *lefty2* and incorrect bilateral and absent *lefty2* expression. (**D**) Quantification of *lefty2* expression sidedness. n is WT = 74, *ntl*$^{-/-}$ = 50, *spaw*$^{-/-}$ = 36, SU5402 = 41, *ntl*$^{-/-}$ + SU5402 = 177, *spaw*$^{-/-}$ + SU5402 = 63. Statistical significance was determined by Chi square analysis. (**A, C**) images are dorsal views, with anterior to the top and left to the reader's left. ns = not significant, *** = p<0.0001.

Figure 2. FGF signaling is necessary for proper CPC migration but not cardiac laterality during jogging. (**A**) Schematization depicting the 18.5-24 hpf SU5402 treatment window during the "Cone Formation and Jogging phase". (**B**) RNA ISH for *myl7* at 24 hpf displaying the stages from cone through extending to correctly jogged heart tubes we see in our treated embryos. (**C**) Quantification of cardiac migration phenotypes. Number of embryos (n) is WT = 686, *ntl*$^{-/-}$ = 152, *spaw*$^{-/-}$ = 171, SU5402 = 531, *ntl*$^{-/-}$ + SU5402 = 117, *spaw*$^{-/-}$ + SU5402 = 146. Statistical significance determined by Chi-square analysis. (**D**) Quantification of heart tube length at 24 hpf. n is WT = 39, *ntl*$^{-/-}$ = 51, *spaw*$^{-/-}$ = 32, SU5402 = 16. Statistical significance determined by Student's t-test. (**E**) RNA ISH for *myl7* at 26.5 hpf visualizing correct left-sided positioning and incorrect midline and right-sided positioning of the heart tube. (**F**) Quantification of cardiac laterality phenotypes. n is WT = 534, *ntl*$^{-/-}$ = 113, *spaw*$^{-/-}$ = 138, SU5402 = 112, *ntl*$^{-/-}$ + SU5402 = 12, *spaw*$^{-/-}$ + SU5402 = 30. Statistical significance determined by Chi-square analysis. (**B, E**) images are dorsal views, with anterior to the top and left to the reader's left. ns = not significant, * = p<0.05, *** = p<0.0001.

Figure 3. FGF signaling promotes CPC migration while Nodal promotes CPC migration and laterality during jogging. (**A**) Schematization of imaging strategy for time-lapse imaging of the cardiac cone throughout jogging, with outer atrial cells in light green and inner ventricular cells in dark green. Left-sided (blue) and right-sided (orange) cells that underwent tracking for analysis are shown. (**B**) Representative time-lapse images depicting cardiac progenitor cell (CPC) migration from the formation of the cardiac cone through the next 3 hours of development. WT and *ntl*$^{-/-}$ embryos typically complete jogging and tube formation in this timeframe. Arrows indicate heart tube direction. Scale = 50 µm. (**C**) Trajectories of left-sided (blue) and right-sided (orange) CPCs during 3 hours of jogging. Scale = 50 µm. (**D**) Rose plots demonstrating the angle of displacement of each tracked left-sided (blue) and right-sided (orange) CPC after 3 hours of jogging. (**E**) Average velocity of left-sided and right-sided CPCs during 3 hours of jogging. Statistical significance determined by Student's t-test. (**C-E**) n = 3 embryos (5 left-sided and 5 right-sided cells tracked per embryo) per condition. (**B-C**) images are dorsal views, with anterior to the top and left to the reader's left. ns = not significant, * = p<0.01.

Figure 4. F-actin dynamics are asymmetric and Nodal-dependent in CPCs during jogging. (**A**) *Tg(myl7:Lifeact-EGFP)* embryo at 24 hpf demonstrating the fluorescence of the CPCs composing the heart tube. (**B**) F-actin protrusive activity in left (blue box) compared to right (orange box) CPCs in the cardiac cone of a *Tg(myl7:Lifeact-EGFP)* embryo over the course of jogging from 19-23 hpf. (**C**) F-actin protrusions (pink asterisks) in a singular CPC of a mosaic *Tg(myl7:Lifeact-EGFP)* embryo at 21 hpf. (**D**) Cardiac cones of *Tg(myl7:Lifeact-EGFP)* embryos, with left-sided (blue oval) and right-sided (orange oval) CPCs marked. (**E**) Schematization of strategy for quantification of fluorescence intensity ratios in the cardiac cone, with the outer atrial cells in light green and the inner ventricular cells in dark green. (**F**) Fluorescence intensity ratio between left-sided and right-sided CPCs. n is WT = 4, *ntl* MO = 4, *spaw* MO = 7, SB-505124 = 5. Statistical significance determined by Student's t-test. (**A-D**) images are dorsal views, with anterior to the top and left to the reader's left. ns = not significant, * = p<0.05.

Figure 5. FGF signaling is necessary for cardiac looping and heart tube extension. (**A**) Schematization depicting the SU5402 treatment windows during the "Elongation phase" from 24-30 hpf, the "Bending phase" from 30-36 hpf, and the "Continuous treatment" window from 24-48 hpf. (**B**) Representative images of vehicle and SU5402-treated *Tg(myl7:EGFP)* embryo hearts at 48 hpf after various SU5402 treatments, depicting how the looping angle is measured (pink lines; AP = anterior/poster axis line and AVC = line through the AVC). (**C**) Quantification of looping angle in vehicle and SU5402-treated hearts at 48 hpf. n is vehicle = 35, SU5402 elongation phase = 30, SU5402 bending phase = 37, *spaw*$^{-/-}$ = 53, *spaw*$^{-/-}$ + SU5402 = 22. Student's t-test. (**D**) Quantification of heart tube length in vehicle and SU5402-treated *Tg(nkx2.5:ZsYellow)* embryo heart tubes at 26.5 or 28 hpf. n is vehicle 26.5 hpf = 24, SU5402 26.5 hpf = 7, vehicle 28 hpf = 13, SU5402 28 hpf = 19. Student's t-test. (**B**) images are ventral views, with anterior to the top and left to the reader's right. ns = not significant, * = p<0.05, ** = p<.001, *** = p<0.0001.

Figure 6. FGF signaling is necessary for proper looping via SHF and necessary for proper AVC development.

(**A**) Representative images of vehicle and *ltbp3* morphants at 48 hpf. (**B**) Quantification of looping angle in vehicle and *ltbp3* morphant hearts at 48 hpf. n is vehicle = 29, MO = 50. Student's t-test. (**C**) RNA ISH for *nppa* in the heart of 48 hpf embryos. WT vehicle-injected embryos have no *nppa* expression in the AVC, while SU5402-injected embryos do (black arrows). (**D**) Quantification of *nppa* expression pattern of 48 hpf hearts. n is vehicle = 22, SU5402 elongation phase = 7, SU5402 bending phase = 18, *spaw*$^{-/-}$ = 15, *spaw*$^{-/-}$ + SU5402 = 13. Chi-square analysis. (**A, C**) images are ventral views, with anterior to the top and left to the reader's right. ns = not significant, *** = p<0.0001.

Supplemental Movies

Movie S1. Live imaging of CPCs jogging in a WT transgenic *Tg(myl7:EGFP)* embryo from the onset of cardiac cone formation until three hours after.

Movie S2. Live imaging of CPCs jogging in a *ntl* mutant *Tg(myl7:EGFP)* embryo from the onset of cardiac cone formation until three hours after.

Movie S3. Live imaging of CPCs jogging in a *spaw* mutant *Tg(myl7:EGFP)* embryo from the onset of cardiac cone formation until three hours after.

Movie S4. Live imaging of CPCs jogging in a SU5402-treated *Tg(myl7:EGFP)* embryo from the onset of cardiac cone formation until three hours after.

Movie S5. Live imaging of CPCs jogging in a *spaw* mutant and SU5402-treated *Tg(myl7:EGFP)* embryo from the onset of cardiac cone formation until three hours after.

Movie S6. Live imaging of F-actin in a WT transgenic *Tg(myl7:Lifeact-EGFP)* embryo from 19-23 hpf, following the cardiac cone as it undergoes jogging.

Movie S7. Live imaging of F-actin in a singular cardiac precursor cell (CPC) from a WT mosaic *Tg(myl7:Lifeact-EGFP)* embryo at 21 hours post fertilization (hpf). Movie is a total of 5 minutes.

Movie S8. Live imaging of F-actin in a *spaw* morphant *Tg(myl7:Lifeact-EGFP)* embryo from 19-23 hpf, following the cardiac cone as it undergoes jogging.

Movie S9. Live imaging of F-actin in a SB-505124-treated *Tg(myl7:Lifeact-EGFP)* embryo from 19-23 hpf, following the cardiac cone as it undergoes jogging.

Movie S10. Live imaging of F-actin in a *ntl* morphant *Tg(myl7:Lifeact-EGFP)* embryo from 19-23 hpf, following the cardiac cone as it undergoes jogging.

Figure 1.

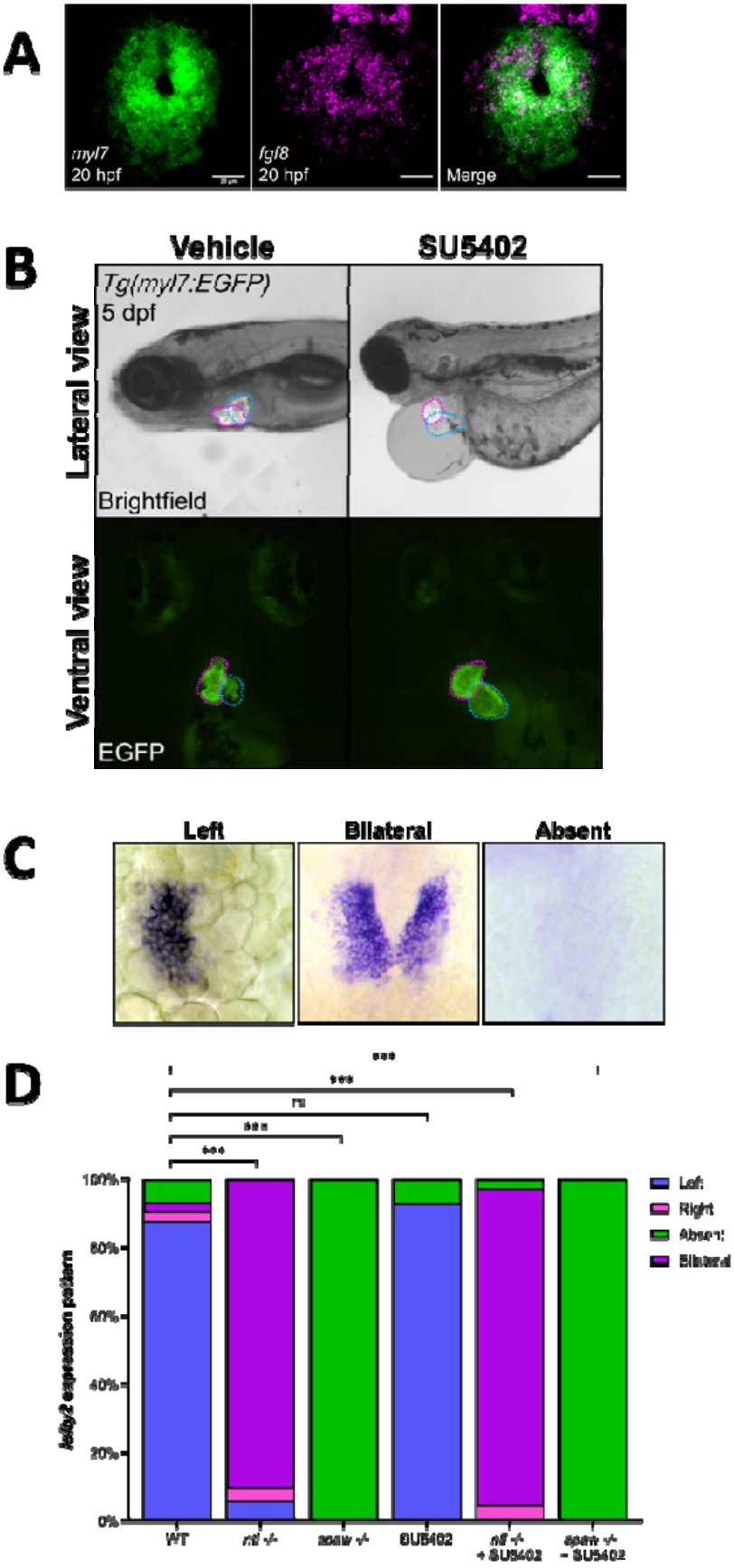
A
myl7
20 hpf
fgf8
20 hpf
Merge
B
Vehicle
SU5402
Tg(myl7:EGFP)
5 dpf
Lateral view
Brightfield
Ventral view
EGFP
C
Left
Bilateral
Absent
D
100%
80%
60%
40%
20%
0%
WT
SU5402
Left
Right
Absent
Bilateral

756

Figure 2.

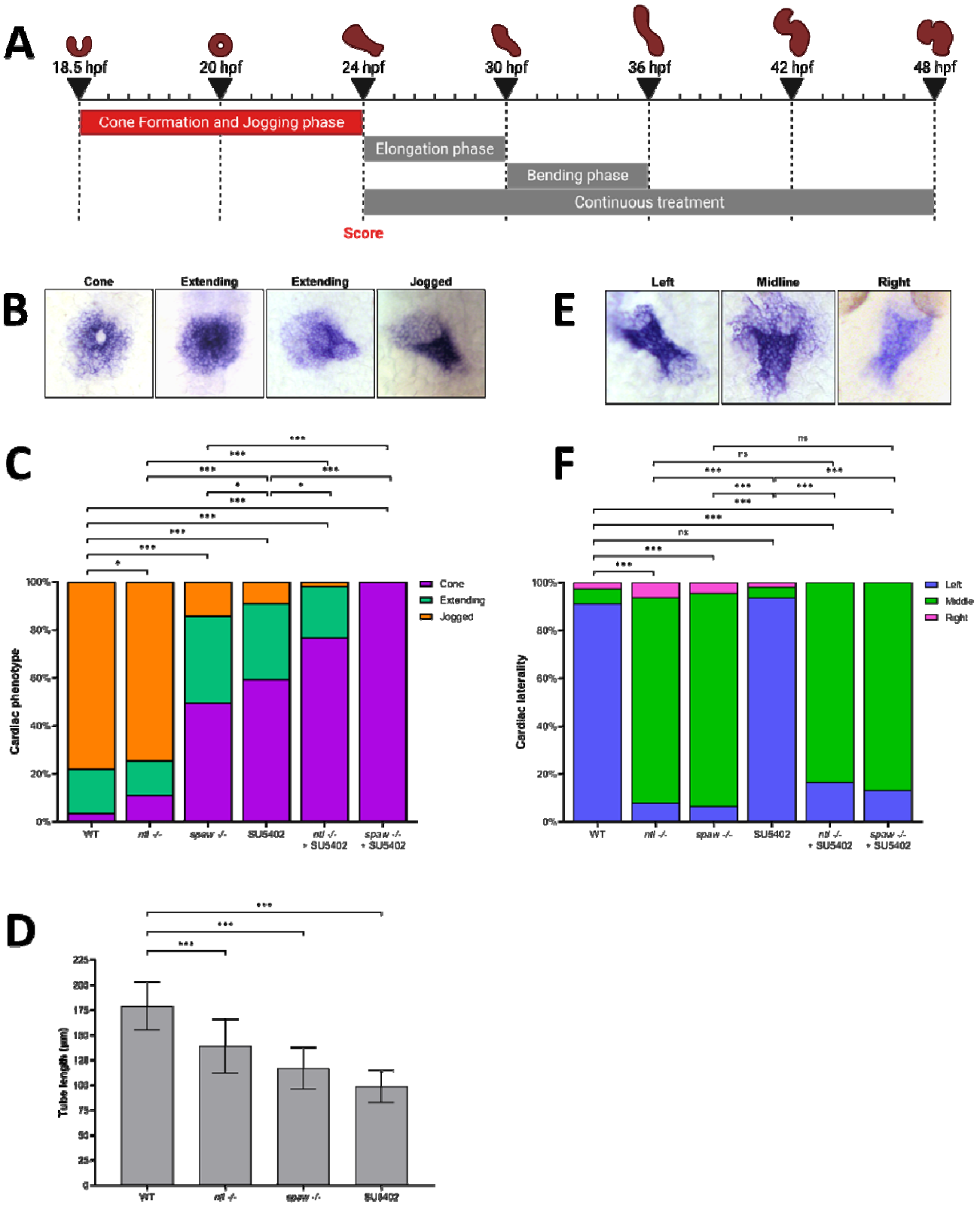
A
18.5 hpf
20 hpf
24 hpf
30 hpf
36 hpf
42 hpf
48 hpf
Cone Formation and Jogging phase
Elongation phase
Bending phase
Continuous treatment
Score
B
Cone
Extending
Extending
Jogged
E
Left
Midline
Right
C
Cardiac phenotype
Cone
Extending
Jogged
WT
ntl -/-
spaw -/-
SU5402
ntl -/- + SU5402
spaw -/- + SU5402
F
Cardiac laterality
Left
Middle
Right
D
Tube length (µm)

Figure 3.

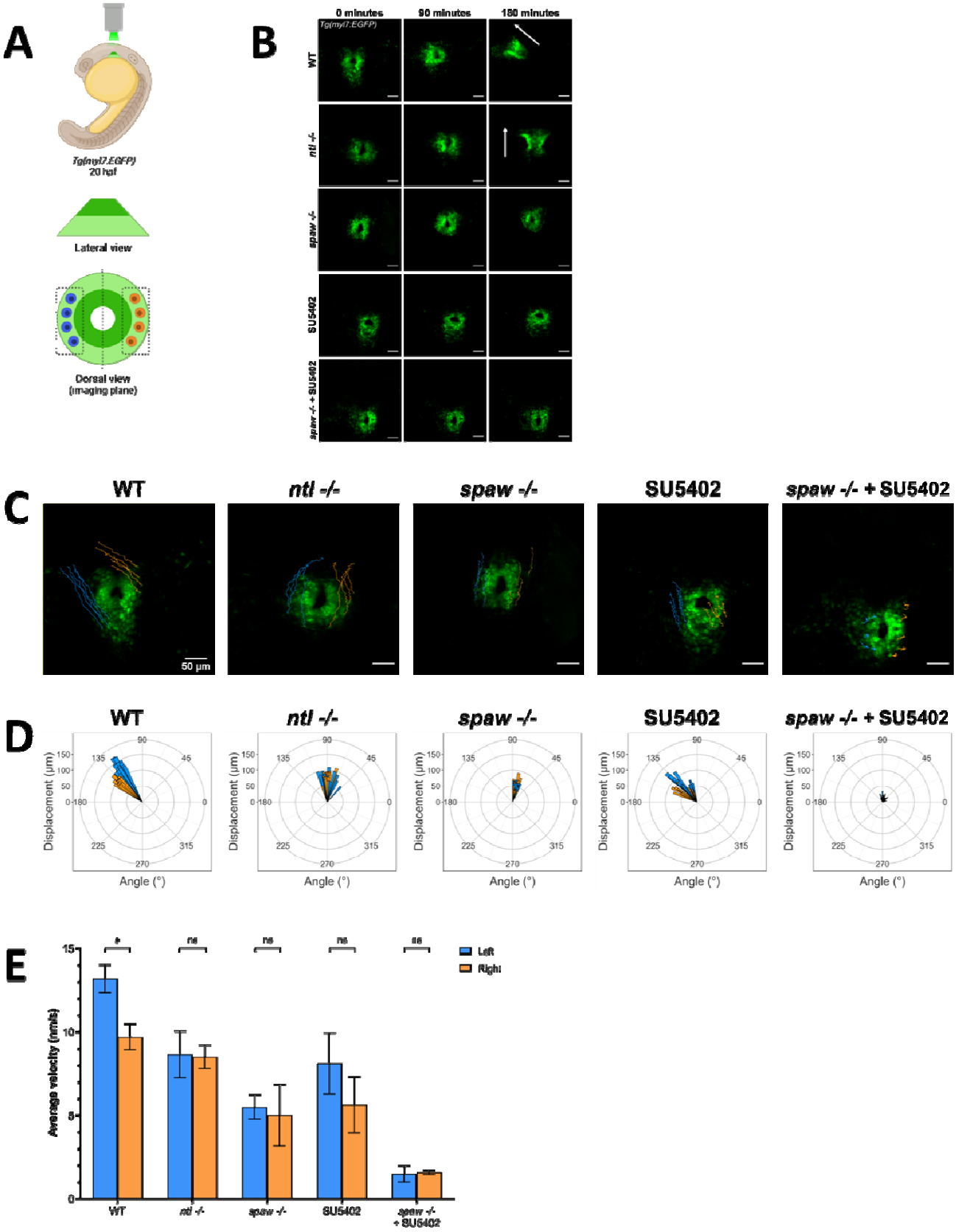

759

760

Figure 4.

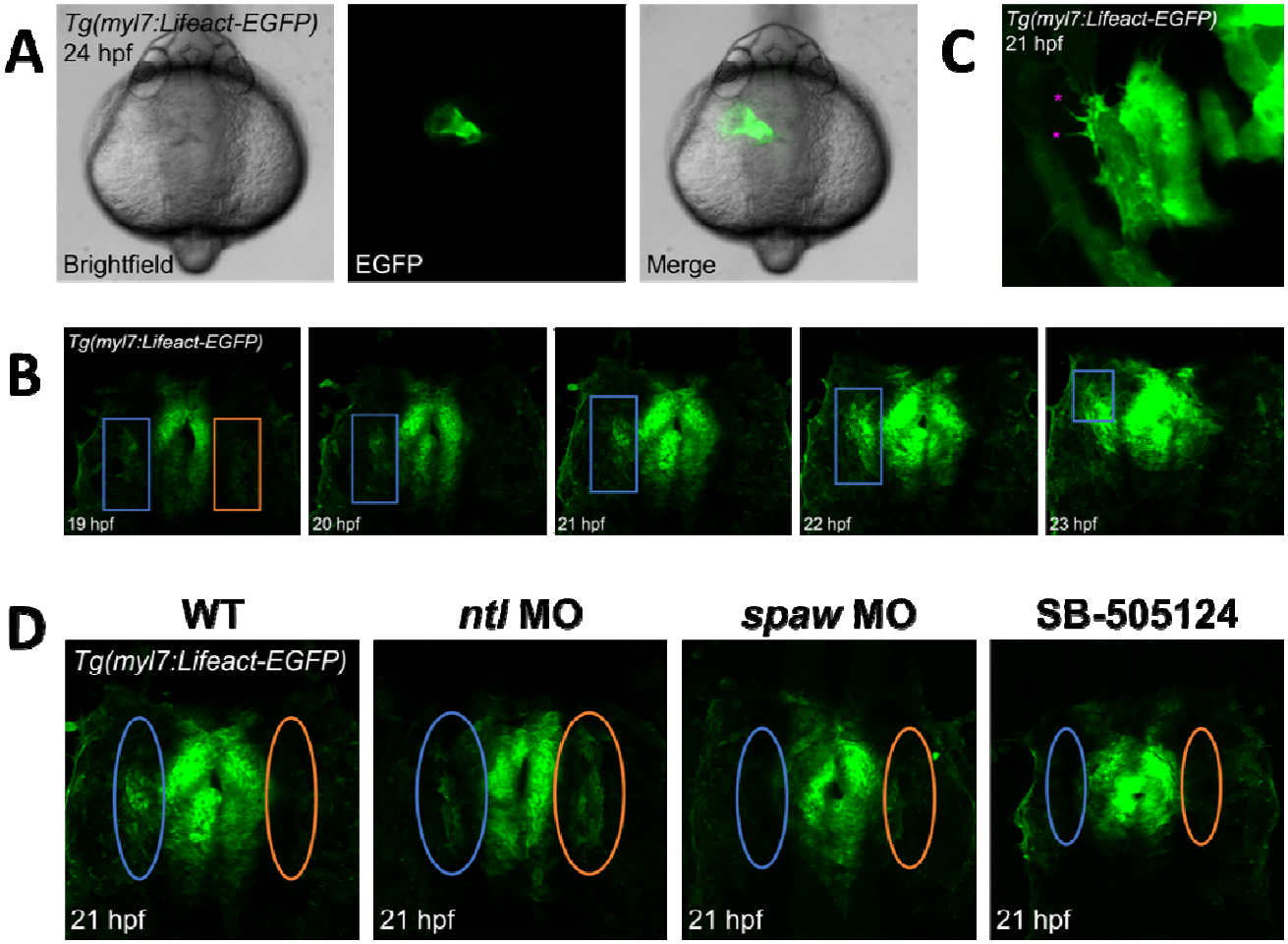

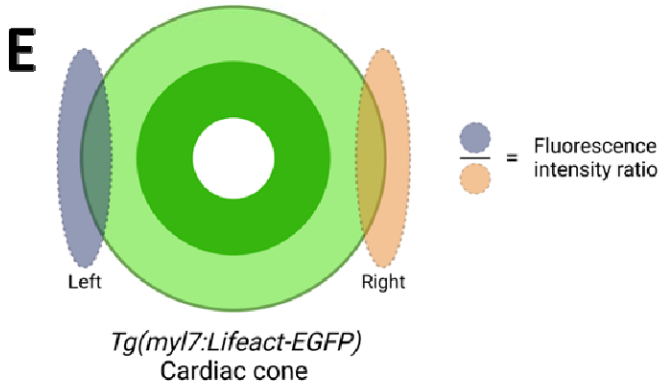

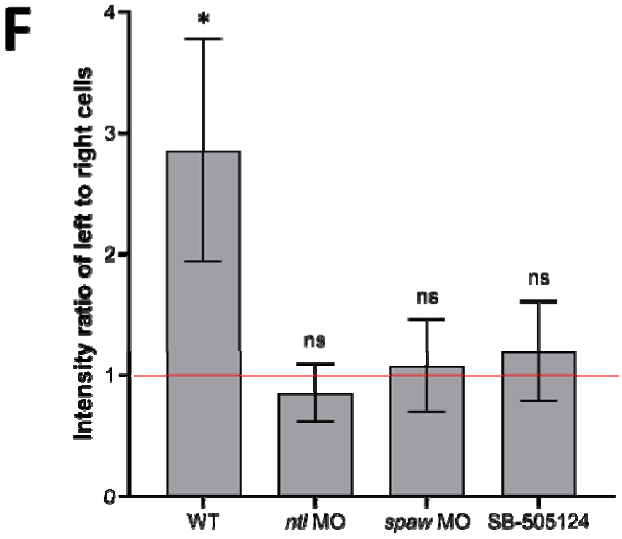

761

762

Figure 5.

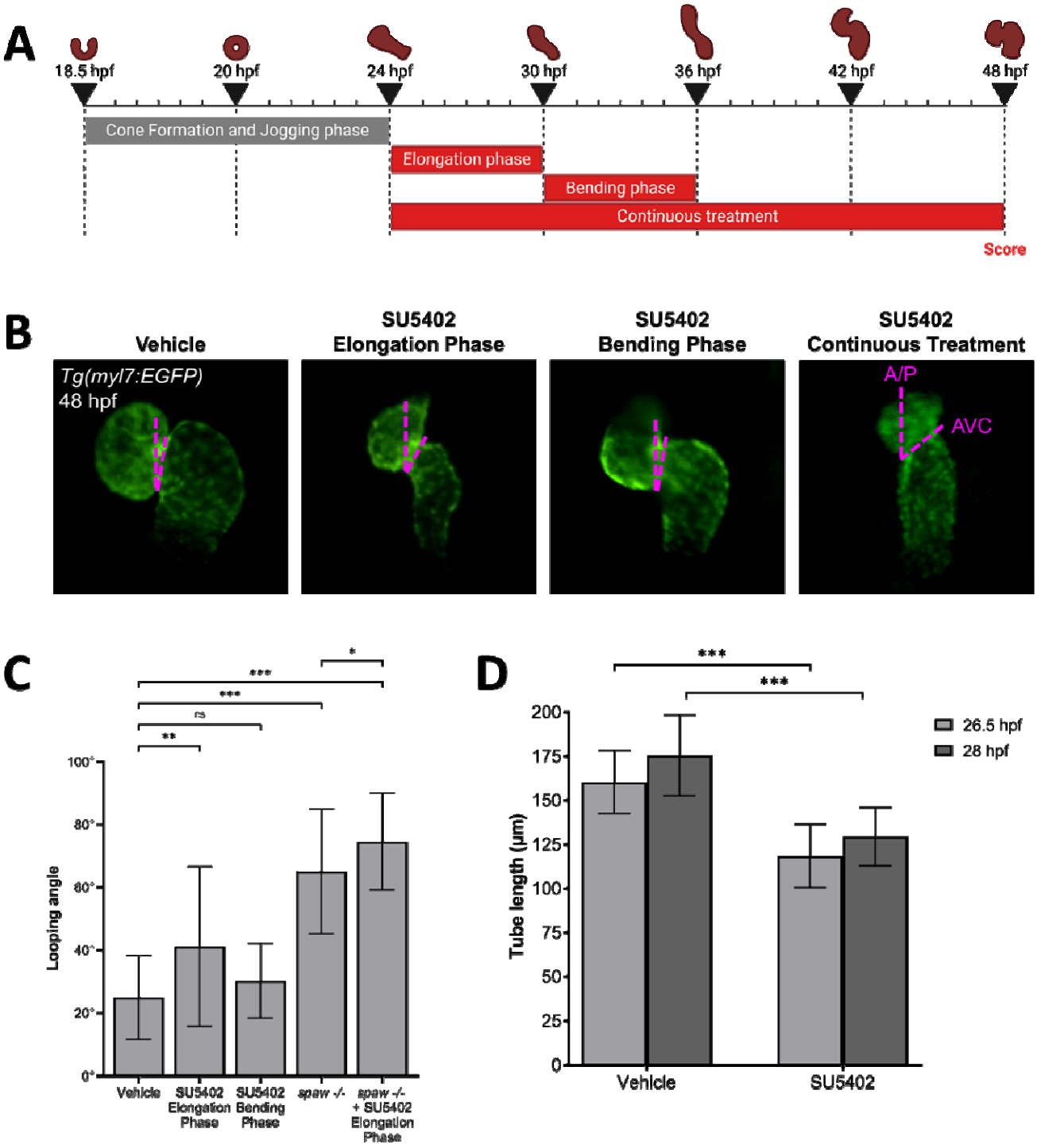

763

764

Figure 6.

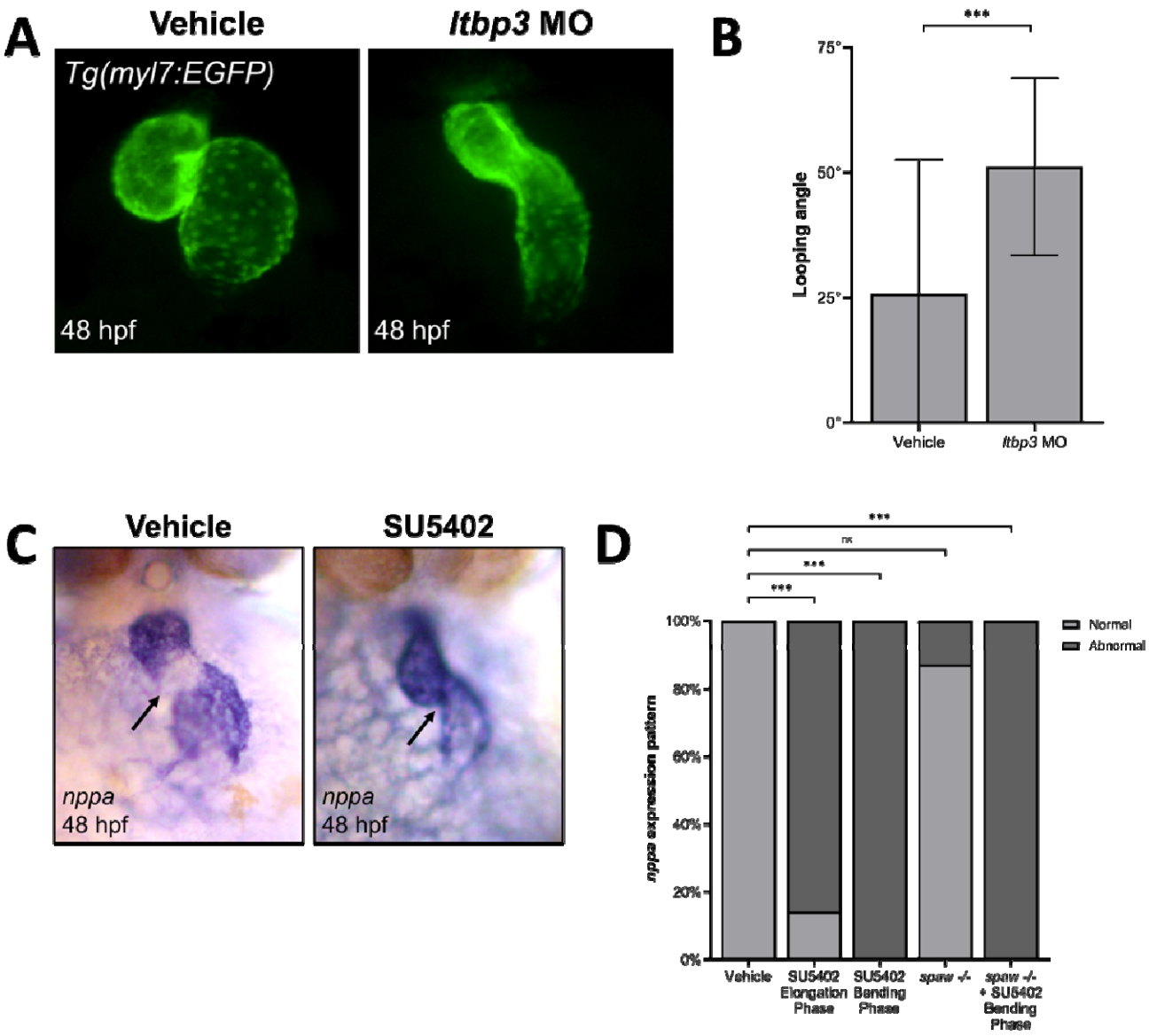

765

766

49 Spadina Ave. Suite 200
Toronto ON M5V 2J1 Canada
www.biorender.com

Confirmation of Publication and Licensing Rights

January 4th, 2024
Science Suite Inc.

Subscription:	*Institution*
Agreement number:	*MI26AS02RF*
Journal name:	*Development*

To whom this may concern,

This document is to confirm that Vanessa Gonzalez has been granted a license to use the BioRender content, including icons, templates and other original artwork, appearing in the attached completed graphic pursuant to BioRender's Academic License Terms. This license permits BioRender content to be sublicensed for use in journal publications.

All rights and ownership of BioRender content are reserved by BioRender. All completed graphics must be accompanied by the following citation: "Created with BioRender.com".

BioRender content included in the completed graphic is not licensed for any commercial uses beyond publication in a journal. For any commercial use of this figure, users may, if allowed, recreate it in BioRender under an Industry BioRender Plan.

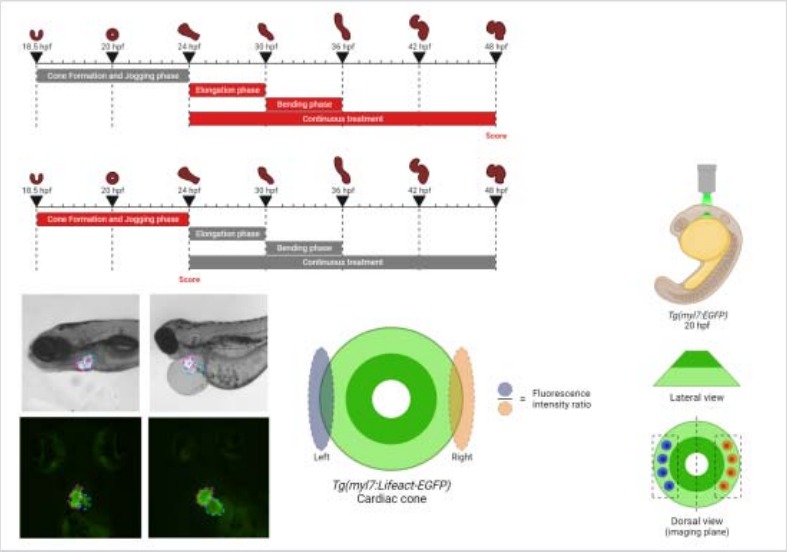

For any questions regarding this document, or other questions about publishing with BioRender refer to our BioRender Publication Guide, or contact BioRender Support at support@biorender.com.